International Journal of Chemical and Biochemical Sciences
(ISSN 2226-9614)

Journal Home page: www.iscientific.org/Journal.html

The Photocatalytic Characteristics of Tin Oxide Nanoparticles Synthesized through *Aquilaria Malaccensis*

Irmaizatussyehdany Buniyamin[1,3*], Noor Asnida Asli[1,3], Mohd Husairi Fadzilah Suhaimi[1,3], Kevin Alvin Eswar[1,3,4], Maryam Mohammad[1,3,5], Mohamad Rusop Mahmood[1,2], Zuraida Khusaimi[1,3*]

[1]NANO-SciTech Laboratory, Centre for Functional Materials and Nanotechnology (FMN), Institute of Science, Universiti Teknologi MARA (UiTM), 40450 Shah Alam Selangor, Malaysia
[2]NANO-ElecTronic Centre, Engineering College, Universiti Teknologi MARA (UiTM), 40450 Shah Alam Selangor, Malaysia
[3]Faculty of Applied Sciences, Universiti Teknologi MARA (UiTM), 40450 Shah Alam Selangor, Malaysia
[4]Faculty of Applied Sciences, Universiti Teknologi MARA (UiTM) Sabah Branch Tawau Campus, 91032 Tawau Sabah, Malaysia
[5]Faculty of Applied Sciences, Universiti Teknologi MARA (UiTM) Perak Branch Tapah Campus, 35000 Tapah Road Perak, Malaysia

Abstract

Nowadays, a significant volume of water is polluted by textile discharges which are known as synthetic dyes. Since synthetic dye molecules do not strongly adhere to fabric, consequently, they are discharged as effluent into the aquatic system. This action degraded the water quality leading to a harmful effect on human health and the environment. Hence, to effectively treat dye-polluted water and prevent all these detrimental effects, a nano-technological approach is required where one of the effective methods for this treatment is the utilization of nanoparticle photocatalysts. In this research work, tin oxide nanoparticles (SnO_2 NPs) were synthesized by applying the green protocol using different concentrations of *Aquilaria malaccensis* leaves. The pure SnO_2 NPs were furnished in an economical, convenient, and non-toxic process contrary to the conventional techniques. Characterizations of SnO_2 NPs using XRD, FTIR, and FESEM indicated the formation of a pure crystalline and tetragonal structure with the bonding of Sn-O-Sn representing anti-symmetric vibration at region 605 to 610 cm^{-1} in a spherical shape. While analysis of HRTEM-SAED revealed a measurement of d-spacing as 0.124 nm, with diffraction rings of (110), (101), and (211) planes corroborating with its tetragonal structure. A reflectance value of 64 % was obtained from UV-DRS analysis, denoting the value of the band gap as 3.12 eV after translation using the Kubelka-Munk formula. In addition, the photocatalytic efficiency was verified under UV irradiation to degrade methylene blue, which resulted in a degradation rate of about 94 % within 70 minutes. These findings have further proven that SnO_2 NPs synthesized using *Aquilaria malaccensis* leaves extract can be of great use in the application of dye-polluted water treatment.

Keywords: Tin oxide nanoparticles, *Aquilaria malaccensis*, Green synthesis, Photocatalytic, Methylene blue.

Full length article **Corresponding Author*, e-mail: *syehdany@uitm.edu.my*, *zurai142@uitm.edu.my*

1. Introduction

Nowadays, a severe problem regarding water mainstream has arisen that relates to toxic wastewater discharge whereby it contains a high amount of synthetic dyes, originally coming from several industries such as fabrics, paper, cosmetics, food and beverages, as well as pharmaceutical [1]. The toxicity effect of synthetic dyes leads to substantial threats not only for humans or living organisms but also for the hydrosphere, in which the undesirable eutrophication process might end up with a damaging result [2]. Synthetic dyes are known to possess low biodegradability. This phenomenon is attributed to their complicated and robust formation, making it difficult to eliminate or separate from the dye-polluted water before discharging [3]. Several techniques, such as physical, and biological methods, have been carried out to resolve this issue precisely to remove the dyes from the effluent.

Unfortunately, the results generated subsequent problems in which the elimination process took a long time to settle and required expensive equipment. Moreover, it was found that the dyes were only partially eliminated, and the worst part was the generation of secondary pollution [4]. The photocatalytic method has been highlighted as the preference for this problem based on the concept of photodegradation of dyes. This method offers excellent efficiency, is easy to handle, safe for users and is environmental-friendly [5]. Regarding this point, an excellent performance of photocatalytic activity using metal oxide nanoparticles for degrading dyes in polluted water has drawn much attention lately [6]. Tin oxide nanoparticles (SnO_2 NPs), a metal oxide semiconductor categorized as an n-type semiconductor with a wide band gap of 3.6 eV, have been highlighted as a potential photocatalyst candidate [7-8]. Its exclusive characteristic, such as high surface-to-volume ratio, chemically stable and low resistivity, has increased sensitivity and adsorption, thus making it appropriate for the photocatalytic process. Other than being a photocatalyst, the excellent characteristics of SnO_2 NPs also led to other beneficial applications such as electrodes, capacitors, lithium-ion batteries, solar cells, gas sensors, and medical [9-14]. The conventional processes to prepare SnO_2 NPs involve chemical and physical methods that require high energy and temperature, expensive operating cost, and employment of hazardous chemicals [15].

These disadvantages contradict the practicality of green-technological. Hence, the replacement must be made with an economical, non-toxic procedure and simple operation. Lately, the green synthesis method has appeared as a new fashion in the research area due to its environmentally friendly approach in which it successfully employed plant extract and only used a non-toxic solvent [16]. The extract produced from several plant segments, such as the leaves, flowers, fruits, seeds and barks, contains several phytochemicals capable of acting as the reducing and capping agent. In this study, the SnO_2 NPs were synthesized from the leaves extract of *Aquilaria malaccensis* (*A. malaccensis*), since the leaves is known to contain a polyphenolic phytochemical that could function to reduce Sn^{4+} of tin precursor during the biosynthesis mechanism [17-19]. The previous report described the green-synthesis of SnO_2 NPs was carried out using *Pruni spinosae flos*, *Psidium guajava*, *Calotropis gigantea*, *Carica papaya*, *Daphne mucronate*, *Aspalathus linearis*, *Pandanus amaryllifolius*, *Citrus aurantifolia*, *Ziziphus jujube*, *Cyphomandra betacea*, *Chromalaena odorata*, *Camellia sinensis*, *Litsea cubeba*, *Brassica oleracea L. var.*, *Phaseolus lunatus L.*, *Tradescantia spathacea*, *Aquilaria malaccensis* and many more [20-36]. In this work, we describe the effect of the leaves extract concentration of *A. malaccensis* towards SnO_2 NPs production under the green synthesis method, as illustrated in **Figure 1**. The morphologies and nanostructures were discussed based on the characterization result from Fourier transform infrared (FTIR), X-ray diffraction (XRD), Field emission scanning electron microscopy (FESEM), High-resolution transmission electron microscopy (HR-TEM), Selected area diffraction (SAED), Energy dispersive X-ray spectroscopy (EDX), UV-Vis and particle sizer analysis. The photocatalytic activity of the most favorable SnO_2 NPs was evaluated in the degradation of organic dyes, namely methylene blue (MB).

2. Methodology

2.1. Materials

In this research study, tin chloride pentahydrate ($SnCl_4.5H_2O$) and methylene blue dye were purchased from Sigma-Aldrich Chemical Company without further purification. The milli-Q water was used throughout the experiments. The leaves of *A. malaccensis* were obtained from the district of Kuala Selangor, Malaysia.

2.2. Preparation of leaves extract

About 80 g of *A. malaccensis* leaves was added to 400 mL of milli-Q water and left to boil at 60°C to 80°C for 20 minutes, followed by filtration. The filtered extract was cooled at room temperature and stored in a refrigerator at 4°C until further use in the synthesis stage.

2.3. Synthesis of SnO_2 NPs

The synthesis procedure for a 1:1 ratio of the leaves extract to salt precursor involved diluting 14.5 ml of *A. malaccensis* leaves extract with 145 ml of milli-Q water. It was added dropwise to 160 ml of $SnCl_4.5H_2O$ (0.05 M) solution. The mixture was left to stir at ambient temperature for 3 hours. Later, centrifugation was carried out to provide a light brown precipitate which was dried at 50ºC overnight. The obtained dried black solid was calcined at 800ºC for 2 hours to furnish pure SnO_2 NPs denoted as OG1 as the outcome. Previous steps were repeated using 29 mL, 44 mL, 59 mL, 73 mL and 87 mL of extracts being diluted in milli-Q water to varying quantities of the extract on the precursor solution for the preparation of OG2 (1:2), OG3 (3:1), OG4 (4:1), OG5 (5:1) and OG6 (6:1), respectively [37].

2.4. Characterization

X-Ray diffraction was operated on PANalytical X'pert PRO using Cu Kα radiation (λ =1.17545Å) at ca. 2θ = 5º to 90º with 45 kV and a scan speed of 0.417782*/sec with 40 mA. The morphology was studied using FESEM brand JEOL model JSM-7600F and HRTEM model JEOL JEM-2100 with a LaB6 filament and operated at an accelerating voltage of 200 kV. UV-visible spectra were analyzed at a wavelength of 200-800 nm using the Varian model of Carry 5000. FTIR spectra were recorded using Perkin Elmer Spectrum 400 in the range 400 to 4000 cm^{-1} by ATR technique. Particle size analysis was conducted using the particle size analyzer brand Malvern model of Zetasizer Nano Series operates at 68mV ±6.8mV.

3. Results and Discussions

3.1. XRD analysis

The diffraction pattern for all synthesized SnO_2 NPs denoting OG1 to OG6 are displayed in **Figure 2.** The diffraction peaks can be indexed to the tetragonal rutile crystalline phase of tin dioxide (JCPDS No: 01-077-0452), which is in accordance with the previous reports [38-39]. The peaks with 2q values at 26.9º, 34.3º, 38.3º, 52.1 º, 55.2º, 58.4º, 62.5º, 65.1º, 66.4º, 71.9 º, 79.2º, and 84.2º are associated with the (110), (101), (200), (211), (220), (002), (310), (112), (301), (202), (321) and (222) planes, respectively.

No alien phase was detected. For SnO_2 NPs with an increased quantity of *A. malaccensis* leaves extract, the XRD patterns presented peaks with a broadening style, suggesting a tendency to become amorphous. The most intense and sharp peaks belong to OG1 attributed to their high order crystallinity and average crystallite size, as the influence of an equal amount of extract and precursor salt used in the green synthesis. Moreover, this might result from the ideal quantity of polyphenol group in *A. malaccensis* leaves extract while reducing and capping Sn^{4+} to Sn^0, suggesting an unnecessarily increased quantity of the extract. Determination of the best possible samples, the examination was arranged on the (110) plane since it is the most-preferred orientation for SnO_2 owing to its richness of atomic density, which can be further analyzed using FESEM and HR-TEM. Additionally, the crystallite sizes of the samples synthesized are calculated using Scherrer's equation based on the (110) plane to give 13.2 nm, 10.5 nm, 8.3 nm, 7.7 nm, 7.70 nm and 6.7 nm for OG1 to OG6, respectively [40-41]. The direction for smaller crystallite size from the additional quantity of extract on precursor solution has also been observed from previous studies, which were during the preparation of SnO_2 NPs using extract of *Camelia sinensis* and *Trigonella foenum-graecum* [42-43].

3.2. FTIR analysis

FTIR analysis was carried out to confirm the presence of the pertinent functional group for SnO_2 NPs construction. The FTIR spectra of the six samples (OG1 to OG6) are displayed in **Figure 3**, showing similar absorption bands. The absorption bands around 605 to 610 cm^{-1} are ascribed to the Sn-O-Sn anti-symmetric vibration. Meanwhile, absorption bands within regions 1000 to 1025 cm^{-1} relate to stretching vibrations of the Sn-OH group due to water molecules absorbed from the environment by SnO_2 NPs [44]. For the above reason, these absorption bands confirmed the formation of SnO_2 NPs and verified the presence of SnO_2 in the crystalline phase.

3.3. FESEM and EDX analysis

Taking the crystallinity and structural characteristics into account, the morphology pattern and the elemental composition of SnO_2 NPs prepared using a ratio of leaves extract: precursor salt solution (1:1, OG1) was investigated. FESEM image of the SnO_2 NPs is presented in **Figure 4**, signifying the morphology of the synthesized SnO_2 NPs that were produced from the equal ratio of *A. malaccensis* leaves extract and precursor salt. This morphological evidence agrees with previous work showing the spherical shape and uniform distribution [45]. The SnO_2 NPs were found to be approximately 27nm. The presence of elemental compositions of O and Sn at 0.5 and 3.5 eV was confirmed by the EDX analysis, in which the elemental percentages of Sn and O were 77.77 % and 22.23 %. Therefore, using the extract of *A. malaccensis* in the green synthesis is a workable technique for producing SnO_2 NPs.

3.4. High-resolution transmission electron microscopy (HRTEM), particle size and selective area electron diffraction (SAED) analyses

The morphology and the shape of OG1 were examined using HRTEM images. The images of SnO_2 NPs exhibit a cluster of nanoparticles with comparatively crystalline, as shown in **Figure 5 (a-b).** The morphology of SnO_2 NPs is spherical, relatively consistent with the FESEM images. In addition, the interplanar distance, which is d-spacing, is measured as 0.124nm corresponding to the (110) plane (**Figure 5c**), befitting to be employed in photocatalysis [46].The agglomeration behavior was recorded by particle size analyzer and is shown in **Figure 6**, demonstrating a confined distribution pattern. The SAED patterns are shown in **Figure 7**, which revealed the diffraction rings that belong to the reflections of (110), (101) and (211) planes, which can be related to the tetragonal structure of the SnO_2 NPs from the XRD analysis.

3.5. UV-Vis diffuse reflectance (UV-DRS) and band gap analysis

The optical characteristic of OG1 was investigated under UV-Vis diffuse reflectance analysis, a non-destructive technique. Figure 8 shows the spectrum of sample OG1, whereby the reflectance value for this pure SnO_2 NPs material was 64% higher than the former reports using *A. malaccensis*, which was 55% [36]. The reflectance result was ascribed to the production of the higher surface-to-volume ratio of SnO_2 NPs, harbouring light scattering and thus encouraging light harvesting [47]. Furthermore, the reflectance value surpassed the recorded value of SnO_2 NPs synthesized using *Plectranthus amboinicus* and *Chromolaena odorata*, recorded at 50 % and 53 %, respectively [48-49]. With this reflectance value, the energy band gaps for SnO_2 NPs produced were calculated using the Kubelka-Munk equation, in which a value of 3.12 eV was found from the expansion of the curve linearity. The values obtained are considered to be comparable to the band gap of SnO_2 NPs synthesized from other plants such as *Calotropis gigantea* (3.1 eV), *Citrus aurantifolia* (3.02 to 3.44 eV), *Averrhoa bilimbi* (3.36 eV) and *Lycopersicon esculentum* (3.4 to 4.1 eV) [50-51].

3.6. Photocatalytic degradation of methylene blue

Photocatalytic activity of the synthesized SnO_2 NPs was analyzed for the degradation of the pollutant dye of Methylene Blue (MB) using a 9-watt UV lamp. The photocatalyst was stirred in 100 ml of methylene blue (15 ppm) for 30 min in the dark to allow adsorption-desorption equilibrium before introducing it to UV irradiation. Within 0 to 10 min intervals, 5 mL of the reaction mixture was taken and centrifuged. The clear supernatant solution was collected and measured using a UV-visible spectrophotometer. The degradation percentage of MB on SnO_2 NPs has been evaluated using the formula 1 [51]. The C_0 and C_t are the concentrations of MB at an initial time and after irradiation.

$$\frac{\frac{C_O}{C_t}}{C_O} \times \mathbf{100} \qquad \textbf{(1)}$$

In regard to dye-polluted water behavior, it was characteristically to has a broad pH scale. Thus, this parameter would characterize the effluent discharge and the generation of OH^- [52]. The pH variation between 3 and 11 was made by adding 0.1 M of HCl and NaOH. From the result, the degradation efficiency of MB using 100 mg of SnO_2 NPs improves by increasing the UV irradiation time (**Figure 9 a**). The degradation of MB was found to be highest

at pH 7, which is at neutral pH, while the degradation rate was recorded low in both acidic and alkaline mediums.

At pH 7, the photocatalytic activity was recorded to be 60 % after 70 minutes of UV irradiation. At the same duration, the degradation was found to be less high in the alkaline solution, while in the acidic condition, it was correspondingly lower. The photocatalytic activity at pH 11 and 3 were recorded as 38% and 8%, which suggested a sequence of pH 7 > pH 11 > pH 3. Hypothetically, the charges of the particle surface can be altered by the pH of the solution, which results in the dispersed condition in the solution [53]. At pH 7, there was no surface charge of SnO_2, and by having Van Der Waals force, the agglomeration between particles was avoided, thus facilitating the dispersal, which led to efficient degradation. For acidic and alkaline solutions, the recombination of generated electron-hole pair was presumably intensified. Both pHs promoted the MB reaction in the solution with the dissolved oxygen into the ground state of the charge transfer compound [54]. The degradation of MB was further characterized by chemical reaction kinetic equations pseudo-first-order kinetic model as shown by **Figure 9 b** [55]. A simplified Langmuir-Hinshelwood (L-H) kinetic model (Equation 2) was applied to define the photocatalytic degradation rate of MB by plotting the graph of -ln(C/C_0) versus time at different pH values [56-57].

$$-ln\frac{C}{C_o} = kt \quad (2)$$

A linear relationship from the plotting furnished the values for the reaction rate constant (k) is higher at neutral conditions, in which the value was found to be 10.9×10^{-3} min^{-1} at pH 7, while 2.9×10^{-3} min^{-1} at pH 11 and 0.5×10^{-3} min^{-1} at pH 3, respectively. Furthermore, the effect of catalyst amount on the MB degradation was investigated by varying the catalyst loading to 100 mg, 200 mg and 300 mg. The loading shows that the highest at 94% resulted from the usage of 300 mg of catalyst greater than using 200 and 100 mg, which represents 71% and 69%, respectively (**Figure 9c**).

The highest degradation was presumably attributed to the availability of the total active surface area, while lower degradation might result from the less catalytic active sites, thus having lower number of reactive species produced under the circumstance of below the optimal catalytic loading [50,58]. The value of k for these catalyst loading was found to be 28.6×10^{-3} min^{-1}, 15.7×10^{-3} min^{-1} and 11.4×10^{-3} min^{-1} for 300 mg, 200 mg and 100 mg, accordingly, as shown in **Figure 9d**. Apart from this, the recyclability of the photocatalyst has been tested for five consecutive cycles, as shown in **Figure 10**. By having this evidence, its capability has been pin-pointed to which extend it has more than 35% degradation for MB and proved to be a robust photocatalyst. The probable photocatalytic degradation mechanism of the MB dye using SnO_2 NPs is clarified by applying the standard protocol as shown in equation 3 to 6 [59-60]. When the SnO_2 NPs surface is irradiated with photon energy either equal to or more significant than its bandgap energy, the formation of holes (h^+) in the valence band and an electron (e^-) in the conduction band are generated. This phenomenon which generates electron-hole pairs, is known as the photo-excitation process. The hole (h^+) acts as an oxidizing agent and oxidizes the pollutant directly or water to form hydroxyl radicals of degraded products. The interaction between e^- and the dissolved oxygen (O_2) resulted in the photo-oxidizing process to give superoxide radicals ($O_2^{\cdot}$). Meanwhile, h^+ leads to photo-reducing H_2O, creating hydroxyl radicals ($OH^{\cdot}$). Superoxide and hydroxyl radicals are highly oxidizing species that escalate the MB degradation giving H_2O and CO_2 as the by-products.

$$SnO_2 + h\nu \rightarrow SnO_2 + e^-_{CB} + h^+_{VB} \ldots\ldots (3)$$

$$e^-_{CB} + O_2 \rightarrow O_2^- \ldots\ldots (4)$$

$$h^+_{VB} + H_2O \rightarrow OH^- \ldots\ldots (5)$$

$$O_2^- \text{ or } OH^- + \text{MB Dye} \rightarrow H_2O + CO_2 + \text{degraded product} \quad (6)$$

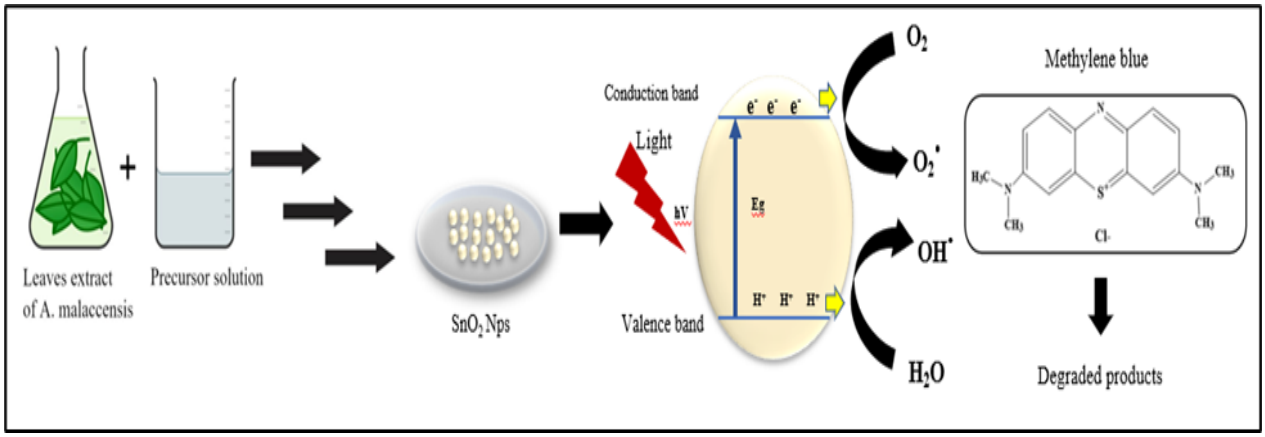

Fig. 1. The illustration of green synthesis of SnO_2 NPs and its application in the photocatalytic process

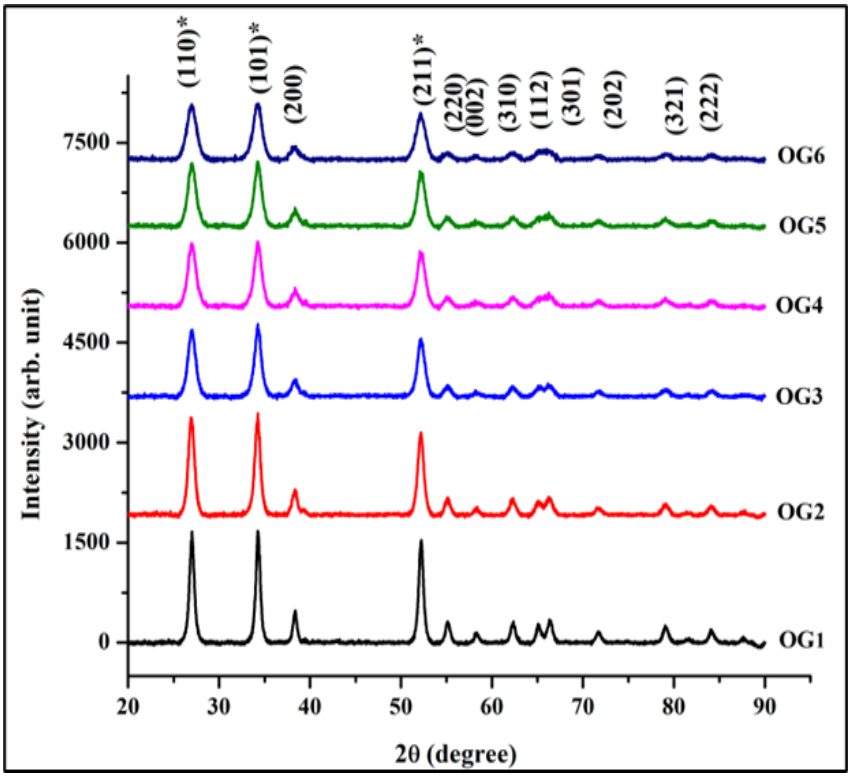

Fig. 2. XRD diffraction patterns for SnO_2 NPs using different extract concentration of *A. malaccensis*.

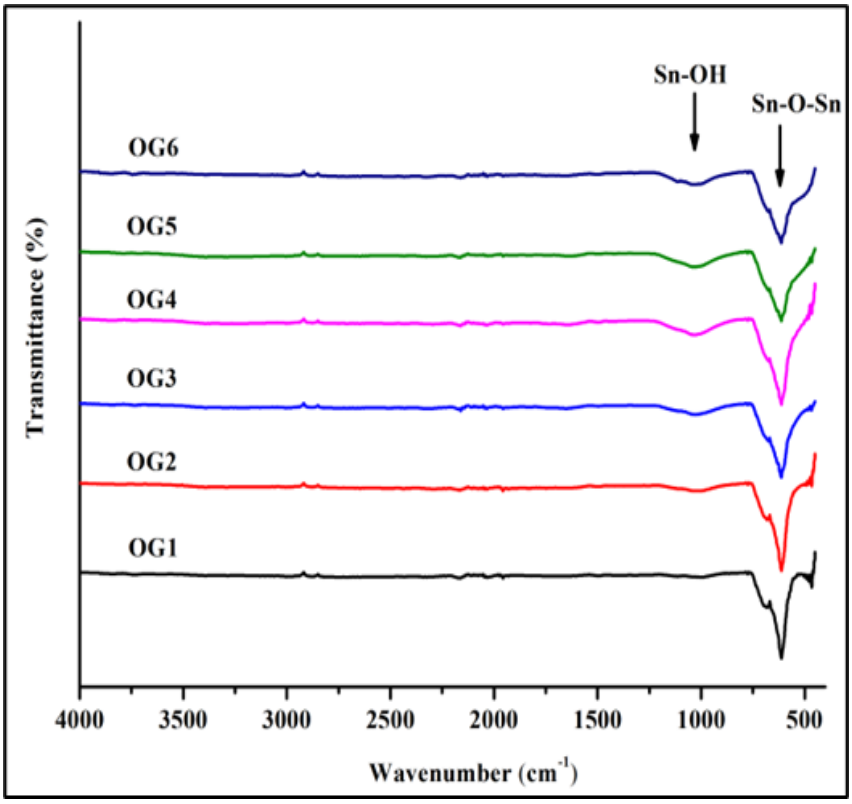

Fig. 3. FTIR spectra of showing the functional groups of SnO_2 NPs.

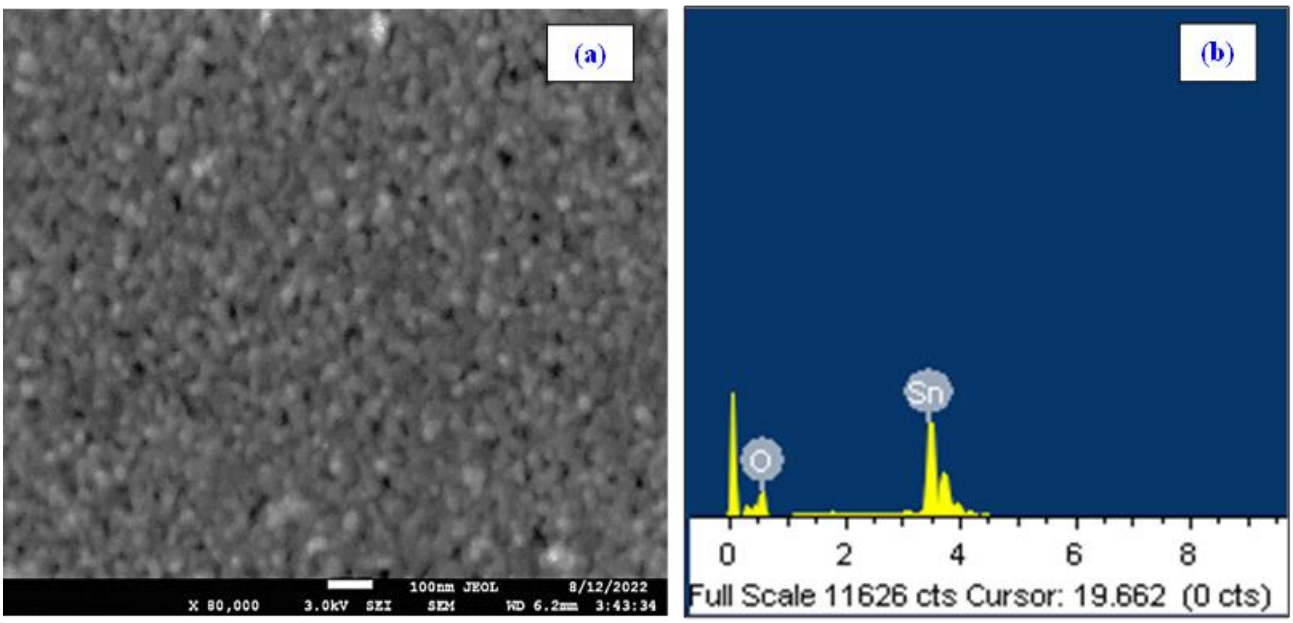

Fig. 4. (a) FESEM image (b) EDX spectrum of SnO_2 NPs.

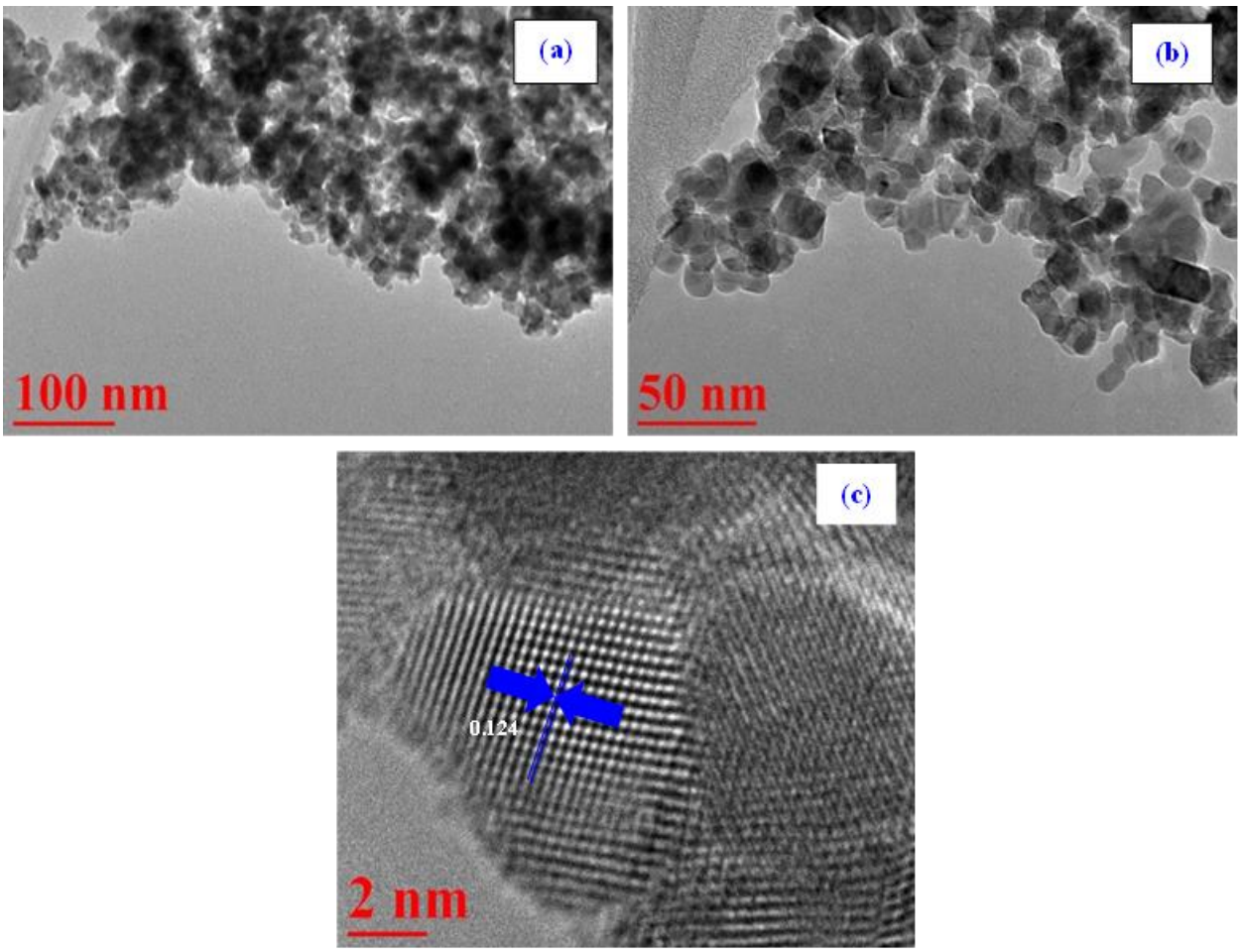

Fig. 5. HRTEM images (a-c) of SnO_2 NPs.

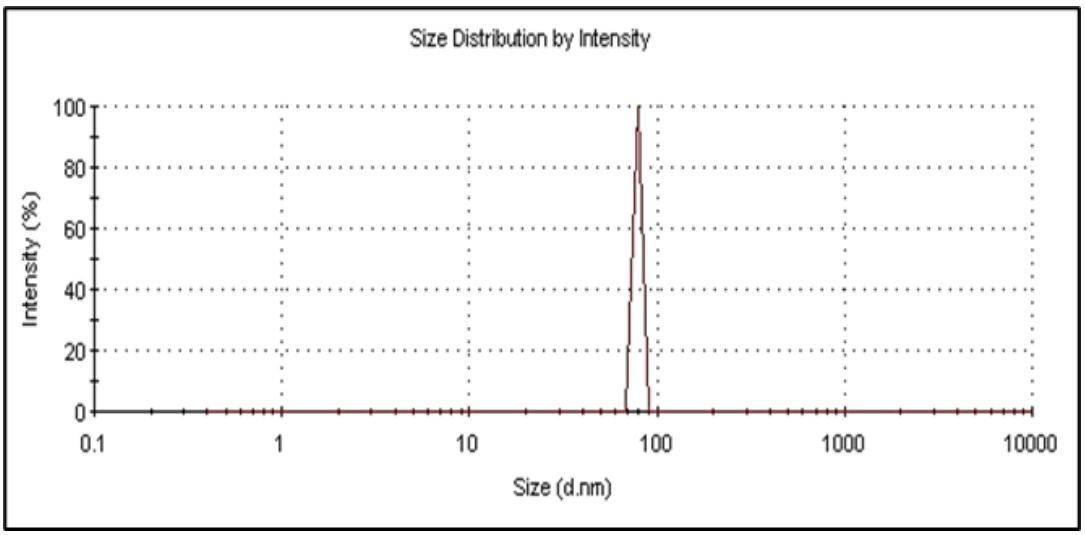

Fig. 6. Particle size distribution of SnO_2 NPs.

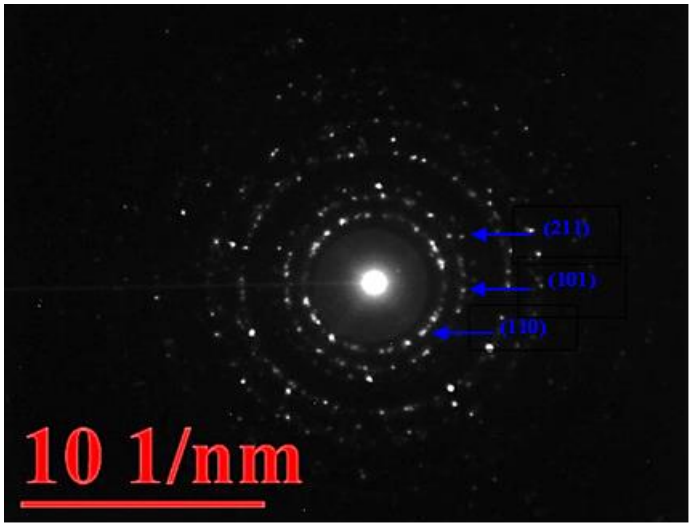

Fig. 7. SAED pattern of SnO_2 NPs.

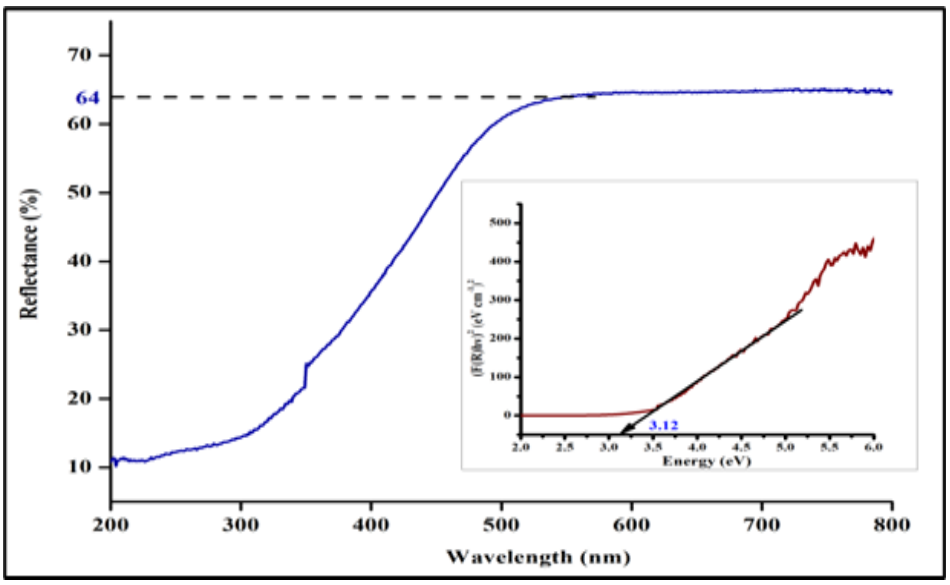

Fig. 8. UV-Vis DRS spectrum and inset is the band gap plot of SnO_2 NPs.

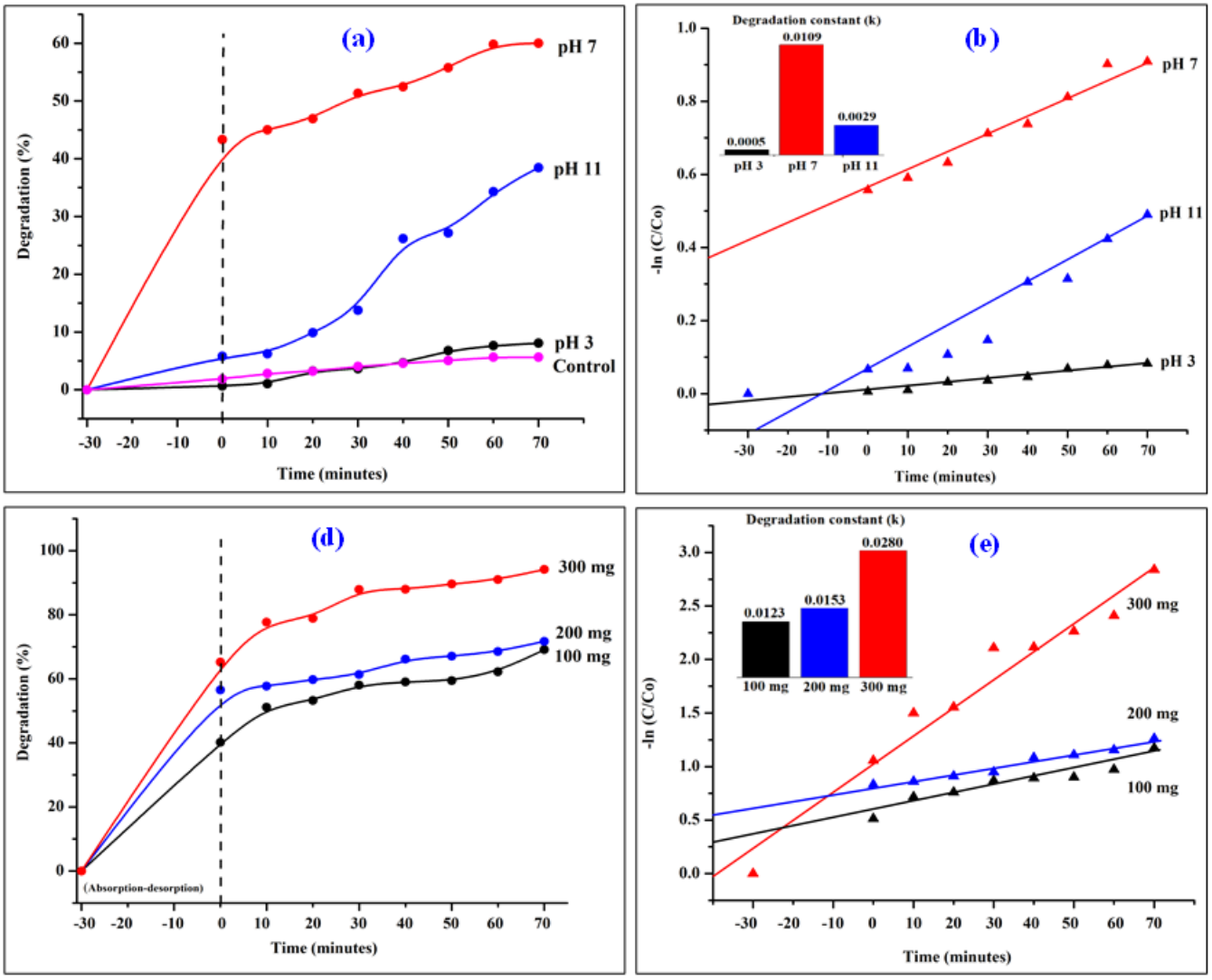

Fig. 9. Photocatalytic evaluation of Methylene Blue solution using SnO_2 NPs.

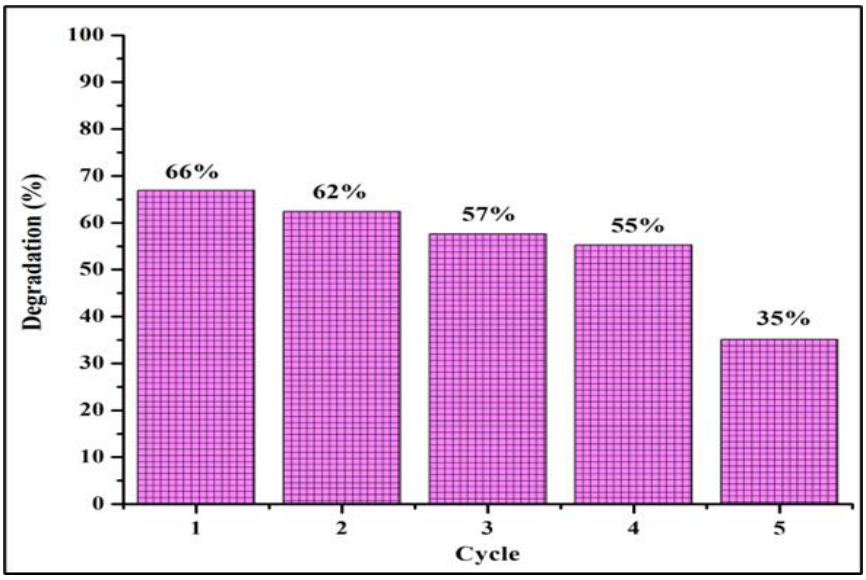

Fig. 10. Photocatalytic cycle of SnO_2 NPs.

4. Conclusions

In this study, a straightforward, non-toxic and effective technique for the green synthesis of SnO_2 NPs was designed via *Aquilaria malaccensis*, and this is the first report on its photocatalytic activity. The ratio of leaf extract to precursor solution influenced the high purity and crystallinity of the synthesized SnO_2 NPs. The photocatalytic activity followed first-order kinetics, presenting 94% degradation of environmental concern methylene blue within 70 minutes, suggesting rich active sites to escalate the photo-excitation. Therefore, the synthesized SnO_2 NPs offer an encouraging solution toward dye-polluted water, which can be benefited to human health, aquatic organism and environment.

References

[1] D. M. Kaur, & R. Sharma. (2022). Recent developments on I and II series transition elements doped SnO_2 nanoparticles and its applications for water remediation process: a review. Journal of Water and Environmental Nanotechnology. 7 (2): 194-217.

[2] I. Ali, O. M. Alharbi, Z. A. Alothman, & A. Y. Badjah. (2018). Kinetics, thermodynamics, and modeling of amido black dye photodegradation in water using Co/TiO_2 nanoparticles. Photochemistry and Photobiology. 94 (5): 935-941.

[3] D. R. Manenti, P. A. Soares, A. N. Modenes, F. R. Espinoza-Quinones, R. A. Boaventura, R. Bergamasco, & V. J. Vilar. (2015). Insights into solar photo-Fenton process using iron (III)–organic ligand complexes applied to real textile wastewater treatment. Chemical Engineering Journal. 266: 203-212.

[4] V. Katheresan, J. Kansedo, & S. Y. Lau. (2018). Efficiency of various recent wastewater dye removal methods: A review. Journal of environmental chemical engineering. 6 (4): 4676-4697.

[5] A. Rafiq, M. Ikram, S. Ali, F. Niaz, M. Khan, Q. Khan, & M. Maqbool. (2021). Photocatalytic degradation of dyes using semiconductor photocatalysts to clean industrial water pollution. Journal of Industrial and Engineering Chemistry. 97: 111-128.

[6] M. Najjar, H. A. Hosseini, A. Masoudi, A. Hashemzadeh, & M. Darroudi. (2020). Preparation of tin oxide (IV) nanoparticles by a green chemistry method and investigation of its role in the removal of organic dyes in water purification. Research on Chemical Intermediates. 46: 2155-2168.

[7] G. Ramanathan, & K. R. Murali. (2022). Photocatalytic activity of SnO_2 nanoparticles. Journal of Applied Electrochemistry. 52 (5): 849-859.

[8] I. Buniyamin, K. A. Eswar, N. A. Asli, M. F. Abd Halim, Z. Khusaimi, & M. R. Mahmood. (2023). Bio-synthesized Tin Oxide Nanoparticles (SnO_2 NPs) as a Photocatalyst Model. Malaysia Journal of Invention and Innovation. 2 (3): 1-5.

[9] E. Yakupova, & G. Ziyatdinova. (2021). Electrode modified with tin (IV) oxide nanoparticles and surfactants as sensitive sensor for hesperidin. Chemistry Proceedings. 5 (1): 54.

[10] K. K. Liu, Q. Jiang, C. Kacica, H. G. Derami, P. Biswas, & S. Singamaneni. (2018). Flexible solid-state supercapacitor based on tin oxide/reduced graphene oxide/bacterial nanocellulose. RSC advances. 8 (55): 31296-31302.

[11] J. A. Weeks, H. H. Sun, H. S. Srinivasan, J. N. Burrow, J. V. Guerrera, M. L. Meyerson, ... & C. B. Mullins. (2019). Facile synthesis of a tin oxide-carbon composite lithium-ion battery anode with high capacity retention. ACS Applied Energy Materials. 2 (10): 7244-7255.

[12] J. Ye, Y. Li, A. A. Medjahed, S. Pouget, D. Aldakov, Y. Liu, & P. Reiss. (2021). Doped bilayer tin (IV) oxide electron transport layer for high open-circuit voltage planar perovskite solar cells with reduced hysteresis. Small. 17 (5): 2005671.

[13] G. Lu, K. L. Huebner, L. E. Ocola, M. Gajdardziska-Josifovska, & J. Chen. (2006). Gas sensors based on tin oxide nanoparticles synthesized from a mini-arc plasma source. Journal of Nanomaterials.

[14] I. Buniyamin, R. M. Akhir, N. A. Asli, Z. Khusaimi, M. F. Malek, & M. R. Mahmood. (2022). Nanotechnology applications in biomedical systems. Current Nanomaterials. 7 (3): 167-180.

[15] P. V. Viet, C. M. Thi, & L. V. Hieu. (2016). The high photocatalytic activity of SnO_2 nanoparticles synthesized by hydrothermal method. Journal of Nanomaterials.

[16] S. Sagadevan, J. A. Lett, I. Fatimah, Y. Lokanathan, E. Léonard, W. C. Oh, ... & M. R. Johan. (2021). Current trends in the green syntheses of tin oxide nanoparticles and their biomedical applications. Materials Research Express. 8 (8): 082001.

[17] B. Wirjosentono, R. Batubara, T. Tamrin, U. Harahap, & D. A. Nasution. (2021). Preparation and phytochemical characterisation of antioxidant active ethanol extract of agarwood (Aquilaria malaccensis Lamk) leaf (EEAL) using liquid chromatography-mass spectroscopy (LC-MS). In AIP Conference Proceedings (Vol. 2342, No. 1). AIP Publishing.

[18] V. V. Gawade, N. L. Gavade, H. M. Shinde, S. B. Babar, A. N. Kadam, & K. M. Garadkar. (2017). Green synthesis of ZnO nanoparticles by using Calotropis procera leaves for the photodegradation of methyl orange. Journal of Materials Science: Materials in Electronics. 28: 14033-14039.

[19] S. Ahmed, S. A. Chaudhry, & S. Ikram. (2017). A review on biogenic synthesis of ZnO nanoparticles using plant extracts and microbes: a prospect towards green chemistry. Journal of Photochemistry and Photobiology B: Biology. 166: 272-284.

[20] R. Dobrucka, J. Dlugaszewska, & M. Kaczmarek. (2018). Cytotoxic and antimicrobial effect of biosynthesized SnO_2 nanoparticles using Pruni spinosae flos extract. Inorganic and Nano-Metal Chemistry. 48 (7): 367-376.

[21] M. Kumar, A. Mehta, A. Mishra, J. Singh, M. Rawat, & S. Basu. (2018). Biosynthesis of tin oxide nanoparticles using Psidium Guajava leave extract for photocatalytic dye degradation under sunlight. Materials Letters. 215: 121-124.

[22] T.T. Bhosale, H.M. Shind, N.L. Gavade, S.B. Babar, V.V. Gawade, S.R. Sabale, R.J. Kamble, B.S. Shirke, K.M. Garadkar. (2018). Biosynthesis of SnO_2 nanoparticles by aqueous leaf extract of *Calotropis gigantea* for photocatalytic applications. J. Mater. Sci. Mater. Electron., 29: 1-10.

[23] D. B. Jadhav, & R. D. Kokate. (2020). Green synthesis of SnO_2 using green papaya leaves for nanoelectronics (LPG sensing) application. Materials Today: Proceedings. 26: 998-1004.

[24] S. Haq, W. Rehman, M. Waseem, A. Shah, A. R. Khan, M. U. Rehman, ... & G. Ali. (2020). Green synthesis and characterization of tin dioxide nanoparticles for photocatalytic and antimicrobial studies. Materials Research Express. 7 (2): 025012.

[25] A. Diallo, E. Manikandan, V. Rajendran, & M. Maaza. (2016). Physical & enhanced photocatalytic properties of green synthesized SnO2 nanoparticles via Aspalathus linearis. Journal of Alloys and Compounds. 681: 561-570.

[26] I. Buniyamin, R. M. Akhir, M. Z. Nurfazianawatie, H. Omar, N. S. A. Malek, N. F. Rostan, ... & M. Rusop. (2023). Aquilaria malaccensis and Pandanus amaryllifolius mediated synthesis of tin oxide nanoparticles: The effect of the thermal calcination temperature. Materials Today: Proceedings. 75: 23-30.

[27] P.A. Luque, O. Nava, C.A. Soto-Robles, H.E. Garrafa-Galvez, M.E. Martinez-Rosas, M.J. Chinchillas-Chinchillas, A.R. Vilchis-Nestor, A. Castro-Beltrán. (2020). SnO_2 nanoparticles synthesized with Averrhoa bilimbi and their performance in photocatalysis. J. Mater. Sci. Mater. Electron., 27: 1-8.

[28] M. Honarmand, M. Golmohammadi, & A. Naeimi. (2019). Biosynthesis of tin oxide (SnO_2) nanoparticles using jujube fruit for photocatalytic degradation of organic dyes. Advanced Powder Technology. 30: 1551-1557.

[29] G. Elango, & S. M. Roopan. (2016). Efficacy of SnO_2 nanoparticles toward photocatalytic degradation of methylene blue dye. Journal of Photochemistry and Photobiology B: Biology. 155: 34-38.

[30] I. Buniyamin, R. M. Akhir, N. A. Asli, Z. Khusaimi, & M. R. Mahmood. (2021). Effect of grinding techniques on Chromolaena odorata leaves for the biosynthesis of SnO_2 nanoparticles. International Journal of Chemical and Biochemical Sciences. 20: 45-52.

[31] J. C. Selvakumari, M. Ahila, M. Malligavathy, & D. P. Padiyan. (2017). Structural, morphological, and optical properties of tin (IV) oxide nanoparticles synthesized using Camellia sinensis extract: a green approach. International Journal of Minerals, Metallurgy, and Materials. 24: 1043-1051.

[32] G. B. Hong, & C. J. Jiang. (2017). Synthesis of SnO_2 nanoparticles using extracts from Litsea cubeba fruits. Materials Letters. 194: 164-167.

[33] J. Osuntokun, D. C. Onwudiwe, & E. E. Ebenso. (2017). Biosynthesis and photocatalytic properties of SnO_2 nanoparticles prepared using aqueous extract of cauliflower. Journal of Cluster Science. 28: 1883-1896.

[34] S. Begum, & M. Ahmaruzzaman. (2018). Green synthesis of SnO_2 quantum dots using Parkia speciosa Hassk pods extract for the evaluation of anti-oxidant and photocatalytic properties. Journal of Photochemistry and Photobiology B: Biology. 184: 44-53.

[35] S. N. Matussin, M. H. Harunsani, A. L. Tan, A. Mohammad, M. H. Cho, & M. M. Khan. (2020). Photoantioxidant studies of SnO_2 nanoparticles fabricated using aqueous leaf extract of Tradescantia spathacea. Solid State Sciences. 105: 106279.

[36] I. Buniyamin, R. M. Akhir, N. A. Asli, Z. Khusaimi, & M. R. Mahmood. (2021). Biosynthesis of SnO_2 nanoparticles by aqueous leaves extract of Aquilaria malaccensis (agarwood). In IOP Conference Series: Materials Science and Engineering (Vol. 1092, No. 1, p. 012070). IOP Publishing.

[37] I. Buniyamin, R.M. Akhir, N.A. Asli, Z. Khusaimi , M.R. Mahmood (2021). Effect of calcination time on biosynthesized SnO_2 nanoparticles using bioactive compound from leaves extract of Chromolaena Odorata. AIP Conf. Proc., 2368: 020006.

[38] S. Sudhaparimala, A. Gnanamani, & A. B. Mandal. (2014). Green synthesis of tin based nano medicine: assessment of microstructure and surface property. American journal of nanoscience and nanotechnology. 2 (4): 75.

[39] G. Elango, S. M. Kumaran, S. S. Kumar, S. Muthuraja, & S. M. Roopan. (2015). Green synthesis of SnO_2 nanoparticles and its photocatalytic activity of phenolsulfonphthalein dye. Spectrochimica Acta Part A: Molecular and Biomolecular Spectroscopy. 145: 176-180.

[40] J. T. Wang, X. L. Shi, W. W. Liu, X. H. Zhong, J. N. Wang, L. Pyrah, ... & K. Tsuri. (2014). Influence of preferred orientation on the electrical conductivity of fluorine-doped tin oxide films. Scientific reports. 4 (1): 3679.

[41] A. Debataraja, D. W. Zulhendri, B. Yuliarto, & B. Sunendar. (2017). Investigation of nanostructured SnO_2 synthesized with polyol technique for CO gas sensor applications. Procedia engineering. 170: 60-64.

[42] P. A. Luque, M. J. Chinchillas-Chinchillas, O. Nava, E. Lugo-Medina, M. E. Martínez-Rosas, A. Carrillo-Castillo, A. R. Vilchis-Nestor, L. E Madrigal-Munoz & H. E. Garrafa-Gálvez. (2021). Green synthesis of tin dioxide nanoparticles using Camellia sinensis and its application in photocatalytic degradation of textile dyes. Optik. 229: 166259.

[43] V. K. Vidhu, & D. Philip. (2015). Phytosynthesis and applications of bioactive SnO_2 nanoparticles. Materials Characterization. 101: 97-105.

[44] E. Gomathi, M. Jayapriya, & M. Arulmozhi. (2021). Environmental benign synthesis of tin oxide (SnO_2) nanoparticles using Actinidia deliciosa (Kiwi) peel extract with enhanced catalytic properties. Inorganic Chemistry Communications. 130: 108670.

[45] S. Matussin, M. H. Harunsani, A. L. Tan, & M. M. Khan. (2020). Plant-extract-mediated SnO_2 nanoparticles: synthesis and applications. ACS Sustainable Chemistry & Engineering. 8 (8): 3040-3054.

[46] A. Bhattacharjee, & M. Ahmaruzzaman. (2015). Photocatalytic-degradation and reduction of organic compounds using SnO_2 quantum dots (via a green route) under direct sunlight. RSC advances. 5 (81): 66122-66133.

[47] L. Fu, Y. Zheng, Q. Ren, A. Wang, & B. Deng. (2015). Green biosynthesis of SnO_2 nanoparticles by plectranthus amboinicus leaf extract their photocatalytic activity toward rhodamine B degradation. Journal of Ovonic Research. 11 (1): 21-26.

[48] I. Buniyamin, R. M. Akhir, N. A. Asli, Z. Khusaimi, & M. Rusop. (2022). Green synthesis of tin oxide nanoparticles by using leaves extract of Chromolaena Odorata: the effect of different thermal calcination temperature to the energy band gap. Materials Today: Proceedings. 48: 1805-1809.

[49] N. Shahzad, N. Ali, A. Shahid, S. Khan, & H. Alrobei. (2021). Synthesis of tin oxide nanoparticles in order to study its properties. Digest Journal of Nanomaterials & Biostructures (DJNB). 16 (1): 41-49.

[50] N. E. Sunny, & V. Kumar. (2019). Biogenesis, characterization and bioefficacy of tin oxide nanoparticles from Averrhoa bilimbi fruit extract. International Journal of Recent Technology and Engineering. 8: 10309-10315.

[51] H. E. Garrafa-Galvez, O. Nava, C. A. Soto-Robles, A. R. Vilchis-Nestor, A. Castro-Beltrán, & P. A. Luque. (2019). Green synthesis of SnO_2 nanoparticle using Lycopersicon esculentum peel extract. Journal of Molecular Structure. 1197: 354-360.

[52] M. H. Abdellah, S. A. Nosier, A. H. El-Shazly, & A. A. Mubarak. (2018). Photocatalytic decolorization of methylene blue using TiO_2/UV system enhanced by air sparging. Alexandria engineering journal. 57 (4): 3727-3735.

[53] M. Abbas. (2021). Factors influencing the adsorption and photocatalysis of direct red 80 in the presence of a TiO_2: equilibrium and kinetics modeling. Journal of Chemical Research. 45 (7-8): 694-701.

[54] H. Yuan, & J. Xu. (2010). Preparation, characterization and photocatalytic activity of nanometer SnO_2. International Journal of Chemical Engineering and Applications. 1 (3): 241-246.

[55] S. Abbasi, & M. Hasanpour. (2017). The effect of pH on the photocatalytic degradation of methyl orange using decorated ZnO nanoparticles with SnO_2 nanoparticles. Journal of materials science: Materials in electronics. 28: 1307-1314.

[56] C. L. Wang. (2018). Fractional kinetics of photocatalytic degradation. Journal of Advanced Dielectrics. 8 (05): 1850034.

[57] V. Goyal, A. Singh, J. Singh, H. Kaur, S. Kumar, & M. Rawat. (2022). Biogenically structural and morphological engineering of Trigonella foenum-graecum mediated SnO_2 nanoparticles with enhanced photocatalytic and antimicrobial activities. Materials Chemistry and Physics. 282: 125946.

[58] Z. Z. Vasiljevic, M. P. Dojcinovic, J. D. Vujancevic, I. Jankovic-Castvan, M. Ognjanovic, N. B. Tadic, ... & M. V. Nikolic. (2020). Photocatalytic degradation of methylene blue under natural sunlight using iron titanate nanoparticles prepared by a modified sol–gel method. Royal Society open science. 7 (9): 200708.

[59] S. K. Kansal, M. Singh, & D. Sud. (2007). Studies on photodegradation of two commercial dyes in aqueous phase using different photocatalysts. Journal of hazardous materials. 141 (3): 581-590.

[60] D. P. Kumar, N. L. Reddy, M. Karthikeyan, N. Chinnaiah, V. Bramhaiah, V. D. Kumari, & M. V. Shankar. (2016). Synergistic effect of nanocavities in anatase TiO_2 nanobelts for photocatalytic degradation of methyl orange dye in aqueous solution. Journal of colloid and interface science. 477: 201-208.